Journal of Materials Chemistry C

PAPER

View Article Online
View Journal | View Issue

Check for updates

Cite this: J. Mater. Chem. C, 2018, 6, 10513

Transforming the molecular orientation of crystalline lamellae by the degree of multi-fluorination within D–A copolymers and its effect on photovoltaic performance†

Jianhong Gao,[a] Wei Wang,[a] Yanqi Hu,[a] Chun Zhan,[a] Shengqiang Xiao, *[a] Xinhui Lu *[b] and Wei You *[ac]

Besides lowering the HOMO energy level of polymer donors to promote higher open circuit voltages (V_{oc}) of polymer solar cells, fluorination of their conjugated backbones has been widely demonstrated to improve the overall device performance as well by inducing face-on orientated polymer crystalline lamellae, which is profitable for vertical charge transport. Nevertheless, over-fluorination (up to 4 fluorine atoms) causes severe solubility reduction and serious segregation, leading to large phase separation of $PC_{71}BM$ and subsequent low and unbalanced charge transport, thus deteriorating J_{sc}, FF and the overall PCE. The underlying impact of multi-fluorination of polymer donors on their interlinked optoelectronic and morphological properties thus remains beyond reach. Guaranteed with sufficient solubility, two D–A copolymers, poly[(5,5′-(2,5-bis((2-octyldodecyl)oxy)-1,4-phenylene)bis(4-fluorothiophene-5,2-diyl))-*alt*-((5-fluorobenzo[*c*][1,2,5]thiadiazole)-4,7-diyl)] (PDTBBT-3F) and poly[(5,5′-(2,5-bis((2-octyldodecyl)oxy)-1,4-phenylene)bis(4-fluorothiophene-5,2-diyl))-*alt*-((5,6-difluorobenzo[*c*][1,2,5]thiadiazole)-4,7-diyl)] (PDTBBT-4F) with 3 and 4 fluorine substituents on the same backbone, respectively, were therefore designed and synthesized. Although lower-lying HOMO energy levels and stronger intermolecular interactions were observed as before, more interestingly, the molecular packing of PDTBBT-3F and PDTBBT-4F in neat films was found to be diametrically opposite. PDTBBT-4F exhibits a preferred face-on orientation whereas the edge-on orientation is dominant for PDTBBT-3F. When mixed with $PC_{71}BM$ to form BHJ blends, the molecular orientation of PDTBBT-3F crystals was transferred to uniform edge-on/face-on intermixing with better crystallinity. Oppositely, the face-on oriented crystals were suppressed to be comparable with edge-on orientated ones with less crystallinity for PDTBBT-4F from the neat film to the BHJ blend. Such distinctive morphology improved the charge generation efficiency, balanced the charge transport and suppressed the charge recombination in the PDTBBT-3F:$PC_{71}BM$ device, eventually leading to an approximate 40% increase of the maximum power conversion efficiency (PCE, 8.33%) in comparison with the PDTBBT-4F:$PC_{71}BM$ device (5.92%). Although the maximum PCE is modest compared with the highest state-of-the-art polymer:fullerene blends, we clearly reveal the effect of the degree of multi-fluorination of polymer donors on their self-assembled thin film structure and photovoltaic properties. Attractive molecular orientation transformation of the crystalline lamellae triggered by the degree of multi-fluorination in this case is likely to percolate into related organic semiconductor fields beyond polymer solar cells.

Received 3rd August 2018,
Accepted 3rd September 2018

DOI: 10.1039/c8tc03872d

rsc.li/materials-c

[a] State Key Laboratory of Advanced Technology for Materials Synthesis and Processing, Wuhan University of Technology, Wuhan, 430070, P. R. China. E-mail: shengqiang@whut.edu.cn
[b] Department of Physics, Chinese University of Hong Kong, Hong Kong, P. R. China. E-mail: xhlu@phy.cuhk.edu.hk
[c] Department of Chemistry, University of North Carolina at Chapel Hill, Chapel Hill, North Carolina 27599-3290, USA. E-mail: wyou@unc.edu

† Electronic supplementary information (ESI) available: General information on materials, measurements and instruments, and device fabrication, ^1H, ^{13}C-NMR and MALDI-TOF mass spectrometry of the compounds, TGA and cyclic voltammogram curves of PDTBBT-3F and PDTBBT-4F, detailed photovoltaic performance optimization, *J–V* curves of electron- and hole-only devices in the dark, and tapping mode AFM images. See DOI: 10.1039/c8tc03872d

Published on 04 September 2018. Downloaded by National Synchrotron Radiation Research on 1/15/2019 1:43:13 AM.

Published on 04 September 2018. Downloaded by National Synchrotron Radiation Research on 1/15/2019 1:43:13 AM.

1. Introduction

Polymer solar cells (PSCs) generally consist of bulk heterojunction (BHJ) blends of an electron-donating polymer and electron-accepting small molecules (fullerenes or non-fullerenes) or polymers, which are cast into thin films from solutions to work as active layers.[1,2] Taking advantage of optimizing their capability for photoelectric conversion by engineering active materials and device architectures, PSCs could offer promising thin, flexible and lightweight devices at low cost.[3–11] There have been notable increases in the performance of PSCs recently with the record PCE approaching 15%.[12–16] In spite of the potential low cost, solution processing raises the challenge of drying the solvent, which greatly impacts the final organization of the components within the BHJ films.[17] The resultant film morphology has been proven to play a crucial role in the overall device performance. In particular, the morphology of BHJ films primarily affects the charge generation efficiency as well as the charge transport and collection efficiency.[6,18] On the other hand, appropriate frontier energy level alignment of the donor and the acceptor within a BHJ blend is of great importance as well, as it helps guarantee sufficient photo-induced electron transfer between components with minimum energy loss.[19] Therefore, molecular structures of active components within a BHJ blend should be engineered such that the blend could form an ideal BHJ morphology with suitable energy distribution to satisfy the requirement for highly efficient photoelectric conversion.[20–23] Embedding this desired electronic property and self-assembly behaviour into the molecular design of active components has remained a grand challenge. Undoubtedly, it requires a profound understanding of fundamental structure–property correlations which are being actively pursued in PSCs.[24]

The chemical strategy of alternating D–A copolymers allows one to fine-tune the energy levels by judicious matching of electron donor (D) and electron acceptor (A) constituents with suitable strength.[25] Numerous D–A copolymers with remarkable photovoltaic performance therefore have been developed as electron donors in polymer:fullerene BHJ PSCs. These achievements have been realized through intensive engineering of the conjugated backbone, and the nature and position of alkyl side chains and substituents in connection with photovoltaic parameters.[7,26–30] Among the possible substitutions of the conjugated backbones, fluorination has demonstrated much success due to the impressive properties of fluorine, such as a van der Waals radius (147 pm) that is only 20% larger than hydrogen (120 pm), the strongest electronegativity possible (4.0), and attractive non-covalent interactions of F$\cdots$H, F$\cdots$S, and F$\cdots\pi$ *etc.*[31–34] These properties effectively endow fluorinated conjugated polymers deeper highest occupied molecular orbital (HOMO) energy levels, more planar backbones and stronger intermolecular π-stacking interactions between polymer chains compared with their non-fluorinated counterparts.[35,36] Temperature-dependent aggregation (TDA), even in diluted solutions, was often observed in them consequently.[31,37] These favourable features, such as fluorination on either the D or A unit or both in D–A copolymers, have prompted fluorinated polymers to be intensively investigated for PSC applications. A number of such reports have shown enhanced V_{oc}, charge generation and transport, and suppressed charge recombination by enhancing the domain purity, reducing the domain size, and improving molecular packing and crystallinity within polymer:fullerene blends.[35,38–40] It's coincident that fluorination often induced an intermixing edge-on/face-on orientation of the polymers within the BHJ blends, which may reduce the transport anisotropy and facilitate effective three-dimensional charge transport.[35,41,42]

Although improved device performance has been frequently attained, the detailed crystal structure and molecular orientation of fluorinated polymers with respect to the device substrates vary from case to case, depending on the chemical structure of the conjugated building blocks as well as on the nature and the position of the solubilizing side chains.[35] For example, Lévêque *et al.* recently suggested that there was a threshold in the length and bulkiness of the grafted alkyl chains to obtain a mixed edge-on/face on molecular orientation for the D–A copolymers composed of fluorinated benzo[*c*][1,2,5]-thiadiazole sandwiched between two thiophene and thieno[3,2-*b*]-thiophene units.[43] The alkyl chains and the fluorination made a complementary contribution to the high PCE of these polymer:$PC_{71}BM$ blends. However, adverse effects on PSC performance were sporadically noticed as well, especially when multiple fluorine atoms (for example, up to 4 of them) were introduced.[44–47] Due to the more increased planarity and non-covalent interactions endowed by over-fluorination, a severe decrease in the solubility and excessive aggregation of the resulting polymers were detected. Consequently, large phase separations with $PC_{71}BM$ were often observed, leading to increased charge recombination and low charge transport with deteriorated device performance. Thus, a balance between incorporating bulky alkyl side chains to assure solution processing and the degree of fluorination has to be addressed to optimize the morphology of the BHJ blends and the overall performance. This cumbersome task has led to less interest in the study of the underlying correlations between self-assembled structures and the photovoltaic performance of multi-fluorinated polymer donors. Providing that the solubility issue can be controlled, the impact of multi-fluorination of D–A copolymers on their interlinked optoelectronic and morphological properties merits further investigation. Additional information on the correlations and further increase in PSC performances could be expected from this effort.

In this respect, we designed two new D–A copolymers consisting of 2,2′-(2,5-bis((2-octyldodecyl)oxy)-1,4-phenylene)-bis(3-fluorothiophene) and 5-fluorobenzo[*c*][1,2,5]thiadiazole or 5,6-difluorobenzo[*c*][1,2,5]thiadiazole (BT) with 3 or 4 fluorine substituents along the same conjugated backbone as indicated in Chart 1. The 1,4-di(thiophen-2-yl)benzene (DTB) backbone was chosen as the electron-donating unit to fluorinate due to the excellent photovoltaic performance of the corresponding D–A copolymers when combined with electron-accepting BT analogues.[48] The two D–A copolymers, namely PDTBBT-3F and PDTBBT-4F with different degrees of multi-fluorination by fluorinating both D and A units, were synthesized to investigate the effects of multi-fluorination on the electronic and

 This journal is © The Royal Society of Chemistry 2018

Published on 04 September 2018. Downloaded by National Synchrotron Radiation Research on 1/15/2019 1:43:13 AM.

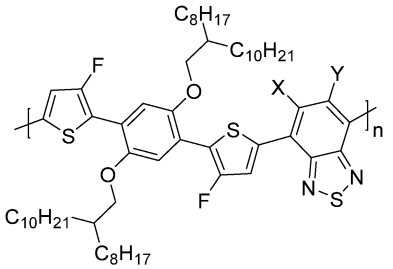

PDTBBT-3F, X=F, Y=H
PDTBBT-4F, X=Y=F

Chart 1 The chemical structures of the two D–A copolymers incorporating 3 or 4 fluorine atoms into the conjugated backbone.

morphological structures and photovoltaic properties of the resulting polymers. Both copolymers present comparable solubility and strong TDA capability in the processing solvent of 1,2-dichlorobenezene (*o*-DCB) when the bulky (2-octyldodecyl)oxy side chain was incorporated. Attractive molecular orientation transformation of the crystalline lamellae triggered by the degree of multi-fluorination was observed in both the neat polymer films and the polymer:$PC_{71}BM$ BHJ blends. PDTBBT-4F exhibits a preferred face-on orientation whereas the edge-on orientation is dominant for PDTBBT-3F. When mixed with $PC_{71}BM$ to form BHJ blends, the face-on orientated PDTBBT-3F crystals increased to coexist almost equivalently with the edge-on orientated ones, resulting in uniform edge-on/face-on intermixing with better crystallinity. For PDTBBT-4F from the neat film to the BHJ blend, on the contrary, the face-on oriented crystals decreased to equivalently coexist with the edge-on orientated ones with less crystallinity. Such morphology transformation rendered a big divergence in the device performance between their corresponding polymer:$PC_{71}BM$ BHJ PSCs. Eventually, an approximate 40% increase of the maximum PCE (8.33%) was achieved for the PDTBBT-3F:$PC_{71}BM$ device in comparison with the PDTBBT-4F:$PC_{71}BM$ device (5.92%), owing to improved charge generation efficiency, balanced charge transport and suppressed charge recombination within the device.

2. Experimental

2.1 General

Information on materials, measurements, instruments, and detailed fabrication and characterization of polymer solar cells can be found in the ESI.†

2.2 Synthesis of monomers and polymers

2,2′-(2,5-Bis((2-octyldodecyl)oxy)-1,4-phenylene)dithiophene (1). To a 25 mL microwave glass vial with a stir bar, 1,4-dibromo-2,5-bis-((2-octyldodecyl)oxy)benzene (4.14 g, 5.0 mmol), 2-(tributylstannyl)thiophene (4.49 g, 12.0 mmol), tetrakis(triphenylphosphine)palladium (115.0 mg, 0.1 mmol), and 15 mL of anhydrous DMF were added in a glove box. The glass vial was then sealed with a cap and heated at 150 °C for 50 minutes in a microwave reactor. After cooling to room temperature, the solvent was removed under reduced pressure. The residue was redissolved in petroleum ether and washed with brine and water subsequently. The organic solution was dried over anhydrous $MgSO_4$, condensed and purified with silica gel column chromatography eluted by petroleum ether to give 3.27 g of the pure product (yield, 78.5%). ^{1}H NMR (500 MHz, $CDCl_3$), δ (ppm): 7.52 (d, J = 3.6 Hz, 2 H), 7.33 (d, J = 5.1 Hz, 2 H), 7.25 (s, 2 H), 7.09 (t, J = 4.4 Hz, 2 H), 3.96 (d, J = 5.4 Hz, 4 H), 1.86–1.91 (m, 2 H), 1.20–1.33 (m, 64 H), 0.88 (t, J = 6.8 Hz, 12 H). ^{13}C NMR (125 MHz, $CDCl_3$), δ (ppm): 149.37, 139.35, 126.63, 125.50, 125.25, 122.92, 112.78, 72.29, 38.17, 31.91, 31.90, 31.47, 30.01, 29.67, 29.64, 29.62, 29.58, 29.34, 29.33, 28.27, 26.88, 26.76, 22.68, 22.67, 17.27, 14.10, 13.57. MALDI-TOF MS for $C_{54}H_{90}O_2S_2$: calcd 834.64, found: 834.7 (M^+).

5,5′-(2,5-Bis((2-octyldodecyl)oxy)-1,4-phenylene)bis(2,4-dibromothiophene) (2). *N*-Bromosuccinimide (2.19 g, 12.3 mmol) was gradually added in the dark to a solution of 2,2′-(2,5-bis((2-octyldodecyl)oxy)-1,4-phenylene)dithiophene (2.50 g, 3.0 mmol) in THF (20 mL). The reaction mixture was refluxed for 2 hours, and after cooling to room temperature, the mixture was extracted with dichloromethane (3 × 20 mL) and washed with sodium carbonate solution and water. The organic layer was dried over anhydrous $MgSO_4$, condensed at reduced pressure and purified with silica gel column chromatography using petroleum ether as the eluent to give 2.92 g of the pure product (yield, 84.9%). ^{1}H NMR (500 MHz, $CDCl_3$), δ (ppm): 7.11 (s, 2 H), 7.01 (s, 2 H), 3.82 (d, J = 5.6 Hz, 4 H), 1.87–1.92 (m, 2H), 1.21–1.34 (m, 64 H), 0.88 (t, J = 6.8 Hz, 12 H). ^{13}C NMR (125 MHz, $CDCl_3$), δ (ppm): 149.97, 135.62, 132.30, 122.30, 116.10, 112.30, 108.74, 72.51, 37.94, 31.92, 31.90, 31.43, 30.01, 29.99, 29.69, 29.63, 29.61, 29.58, 29.35, 28.26, 28.17, 26.83, 26.75, 22.68, 17.27, 14.11, 13.57. MALDI-TOF MS for $C_{54}H_{86}Br_4O_2S_2$: calcd 1146.28, found: 905.7 ($(M - 3Br)^+$).

2,2′-(2,5-Bis((2-octyldodecyl)oxy)-1,4-phenylene)bis(3-bromothiophene) (3). A solution of 2.4 M of *n*-BuLi in hexane (1.8 mL, 4.4 mmol) was added dropwise to the solution of compound **2** (2.29 g, 2.0 mmol) in anhydrous THF (12.0 mL) at −78 °C under nitrogen. After stirring for 30 min, 0.23 mL of methanol (6.0 mmol) was added into the mixture. The reaction mixture was then quenched with water and the resultant mixture was extracted with petroleum ether, and dried over $MgSO_4$. After the removal of solvent by rotary evaporation, the crude product was further purified by silica gel column chromatography with petroleum ether as the eluent to afford 1.61 g of the product (yield, 83.1%). ^{1}H NMR (500 MHz, $CDCl_3$), δ (ppm): 7.34 (d, J = 5.4 Hz, 2H), 7.13 (s, 2H), 7.05 (d, J = 5.4 Hz, 2H), 3.82 (d, J = 5.5 Hz, 4H), 1.68–1.73 (m, 2H), 1.20–1.35 (m, 64H), 0.89 (t, J = 6.9 Hz, 12H). ^{13}C NMR (125 MHz, $CDCl_3$), δ (ppm): 150.18, 134.15, 130.18, 125.71, 122.84, 116.61, 109.75, 72.35, 37.99, 31.93, 31.92, 31.36, 30.01, 29.69, 29.65, 29.62, 29.57, 29.35, 26.79, 22.69, 22.68, 14.12. MALDI-TOF MS for $C_{54}H_{88}Br_2O_2S_2$: calcd 990.46, found: 909.7 ($(M - Br)^+$).

2,2′-(2,5-Bis((2-octyldodecyl)oxy)-1,4-phenylene)bis(3-fluorothiophene) (4). To a flask containing compound **3** (1.49 g, 1.5 mmol) and 10 mL of anhydrous THF, 2.4 M of *n*-BuLi in hexane (1.25 mL, 3.0 mmol) was added dropwise to the flask

Published on 04 September 2018. Downloaded by National Synchrotron Radiation Research on 1/15/2019 1:43:13 AM.

cooled to −78 °C under N_2. After stirring for 50 minutes at −78 °C, a solution of *N*-fluorobenzenesulfonimide (0.99 g, 3.3 mmol) in 20 mL of THF was added. The reaction was stirred overnight at room temperature and then quenched with water, extracted with dichloromethane, and dried over $MgSO_4$. After the removal of solvent by rotary evaporation, the crude product was further purified by silica gel column chromatography with petroleum ether as the eluent to afford 0.78 g of the product (yield, 59.6%). ^{1}H NMR (500 MHz, $CDCl_3$), δ (ppm): 7.40 (s, 2H), 7.19 (dd, J = 5.4, 4.1 Hz, 2H), 6.86 (d, J = 5.6 Hz, 2H), 3.92 (d, J = 5.5 Hz, 4H), 1.80–1.86 (m, 2H), 1.20–1.35 (m, 64H), 0.88 (t, J = 6.9 Hz, 12H). ^{13}C NMR (125 MHz, $CDCl_3$), δ (ppm): 156.04, 153.97, 149.20, 123.57, 119.91, 116.89, 113.61, 72.38, 38.09, 31.93, 31.92, 31.41, 30.01, 29.68, 29.65, 29.62, 29.52, 29.35, 29.33, 26.83, 26.13, 22.69, 22.68, 14.10. ^{19}F NMR (940 MHz, $CDCl_3$), δ (ppm): −128.01 (d, J = 7.6 Hz, 2F). MALDI-TOF MS for $C_{54}H_{88}F_2O_2S_2$: calcd 870.62, found: 870.8 (M^+).

(5,5′-(2,5-Bis((2-octyldodecyl)oxy)-1,4-phenylene)bis(4-fluorothiophene-5,2-diyl))bis-(trimethylstannane) (5). A 2.4 M solution of *n*-BuLi in hexane (1.0 mL, 2.4 mmol) was added to a flame-dried flask containing compound **4** (0.87 g, 1.0 mmol) and 8 mL of anhydrous THF at −78 °C under N_2. After stirring for 30 min at −78 °C, the solution was allowed to warm to room temperature while stirring for another 30 min. The solution was then cooled to −78 °C again, and a 1 M solution of trimethyltin chloride in hexane (2.6 mL, 2.6 mmol) was added. The reaction was stirred overnight at room temperature and then quenched with water, extracted with diethyl ether, and dried over $MgSO_4$. After removal of the solvent under reduced pressure, the product (1.14 g, yield 95%) was obtained as a pale-yellow liquid and used without further purification. ^{1}H NMR (500 MHz, $CDCl_3$), δ (ppm): 7.36 (s, 2H), 6.92 (s, 2H), 3.91 (d, J = 5.4 Hz, 4H), 1.76–1.85 (m, 2 H), 1.20–1.35 (m, 64H), 0.88 (t, J = 6.9 Hz, 12H), 0.39 (s, 18H). ^{13}C NMR (125 MHz, $CDCl_3$), δ (ppm): 157.65, 155.45, 149.23, 124.22, 122.13, 120.10, 113.06, 72.38, 38.21, 31.94, 31.60, 31.47, 30.13, 29.72, 29.68, 29.63, 29.37, 26.96, 22.70, 22.66, 22.62, 14.11, 11.42, −8.41. ^{19}F NMR (940 MHz, $CDCl_3$), δ (ppm): −129.62 (s, 2F). MALDI-TOF MS for $C_{60}H_{104}F_2O_2S_2Sn_2$: calcd 1196.55, found: 1196.7 (M^+).

Poly[(5,5′-(2,5-bis((2-octyldodecyl)oxy)-1,4-phenylene)bis(4-fluorothiophene-5,2-diyl))-*alt*-((5-fluorobenzo[*c*][1,2,5]thiadiazole)-4,7-diyl)] (PDTBBT-3F). To a 50 mL two-neck round-bottom flask was charged **5** (0.36 g, 0.3 mmol), 4,7-dibromo-5-fluorobenzo[*c*][1,2,5]thiadiazole (0.094 g, 0.3 mmol), $Pd_2(dba)_3$ (8.2 mg, 0.009 mmol), tri(*o*-tolyl)phosphine (16.0 mg, 0.054 mmol), and anhydrous chlorobenzene (8.0 mL) under nitrogen. After being transferred out of the glove box, the reaction mixture was heated at reflux for 48 hours under the protection of N_2. Then, the reaction mixture was cooled down to room temperature and precipitated by dropwise addition into methanol. The solid was collected by filtration and then the crude product was purified by Soxhlet extraction with methanol, acetone, hexane, dichloromethane and chloroform sequentially. The fraction in chloroform was concentrated and precipitated in 15 mL of methanol, and then the resulting solid was filtered and dried under vacuum to obtain 0.21 g of the final polymer (yield, 70.1%). GPC: M_n = 26.72 kg mol^{-1}, M_w = 53.94 kg mol^{-1}, PDI = 2.02. A resolvable ^{1}H NMR spectrum of the copolymer was not obtained due to its strong aggregation in $CDCl_3$ solution at room temperature for NMR testing.

Poly[(5,5′-(2,5-bis((2-octyldodecyl)oxy)-1,4-phenylene)bis(4-fluorothiophene-5,2-diyl))-*alt*-((5,6-difluorobenzo[*c*][1,2,5]-thiadiazole)-4,7-diyl)] (PDTBBT-4F). The polymer was prepared according to the same procedure for PDTBBT-3F from compound **5** (0.36 g, 0.3 mmol), 4,7-dibromo-5,6-difluorobenzo[*c*]-[1,2,5]thiadiazole (99.0 mg, 0.3 mmol), $Pd_2(dba)_3$ (8.2 mg, 0.0090 mmol), tri(*o*-tolyl)phosphine (16.0 mg, 0.054 mmol), and anhydrous chlorobenzene (8.0 mL) with a yield of 85.0% (0.26 g). GPC: M_n = 23.14 kg mol^{-1}, M_w = 50.12 kg mol^{-1}, PDI = 2.16. Similarly, the ^{1}H NMR spectrum of PDTBBT-4F could not be gained due to its strong aggregations in $CDCl_3$ solution.

3. Results and discussion

3.1 Synthesis and thermal properties of the polymers

As shown in Scheme 1, the fluorinated electron-donating monomer and both D–A copolymers of PDTBBT-3F and PDTBBT-4F were synthesized. Two long branched chains of (2-octyldodecyl)oxy groups were grafted onto the central benzene ring to ensure sufficient solubility of the resulting polymers in common organic solvents for solution processing, such as toluene, chlorobenzene, *o*-dichlorobenzene, *etc.* Compound **1** was synthesized by a Stille coupling reaction between 1,4-dibromo-2,5-bis((2-octyldodecyl)oxy)benzene and 2-(tributylstannyl)thiophene with $Pd(PPh_3)_4$ as the catalyst in DMF, and then brominated with *N*-bromosuccimide (NBS) to obtain tetra-brominated monomer **2**. The dibrominated compound of **3** was subsequently prepared through *n*-butyllithium (*n*-BuLi). Further lithiation by *n*-BuLi and then quenching with *N*-fluorobenzenesulfonimide (NFSI) in THF provide compound **4**, which was converted into compound **5** as a distannylated monomer for polymerization by a standard stannylation. Finally, the two target D–A copolymers were synthesized *via* a typical Stille-coupling reaction of **5** with fluorinated BT analogues of compounds **6** and **7**, respectively, catalyzed by $Pd_2(dba)_3$/P-(*o*-tol)$_3$ in refluxed chlorobenzene under N_2. All compounds were purified by silica gel column chromatography, and their structures and purity were verified by ^{1}H NMR, ^{13}C NMR, and matrix-assisted laser desorption ionization time-of-flight (MALDI-TOF) MS, and the corresponding spectra are shown in the ESI.† Both the D–A copolymers were purified by Soxhlet extraction and the fraction in chloroform was collected and used for further investigation. PDTBBT-3F and PDTBBT-4F offer similar solubility in chlorobenzene (11.5 and 10.2 mg mL^{-1}, respectively) and in *o*-dichlorobenzene (15.6 and 14.5 mg mL^{-1}, respectively). Although non-symmetrical BTs with mono-fluorination were introduced in PDTBBT-3F, the relatively even distribution of fluorine atoms along the whole polymer backbone could still be realized. Since both copolymers exhibit strong aggregation behaviour at room temperature (refer to UV-vis absorption spectra below) in solution, the number-average molecular weight (M_n) and the weight-average molecular weight

 This journal is © The Royal Society of Chemistry 2018

Published on 04 September 2018. Downloaded by National Synchrotron Radiation Research on 1/15/2019 1:43:13 AM.

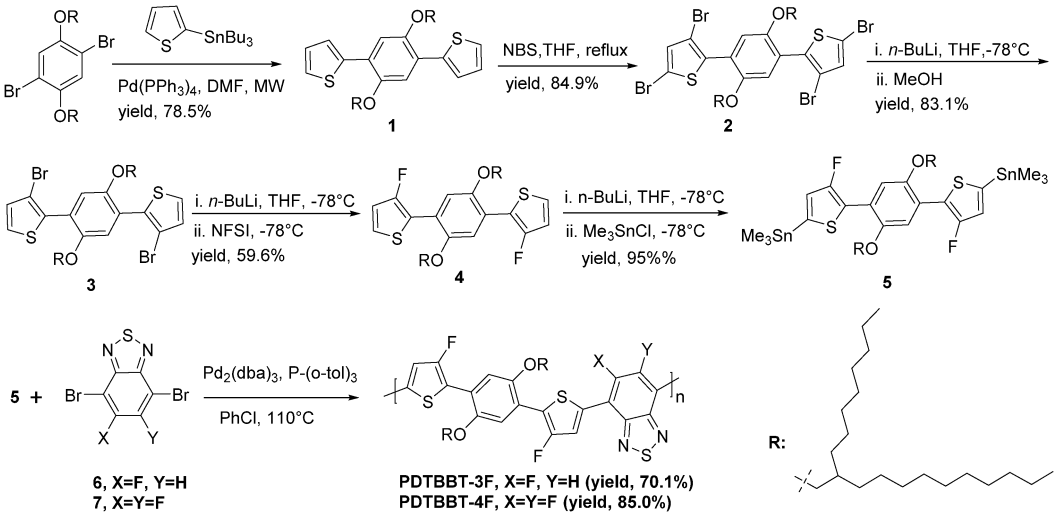

Scheme 1 Synthetic routes of the fluorinated electron-donating monomers and their D–A copolymers of PDTBBT-3F and PDTBBT-4F.

(M_w) were obtained by high-temperature gel-permeation chromatography (GPC) using 1,2,4-trichlorobenzene as the eluent at 150 °C. M_n and M_w were found to be 26.7 and 53.9 kg mol^{-1}, respectively, with a polydispersity index (PDI) of 2.02 for PDTBBT-3F, and 23.1 and 50.1 kg mol^{-1}, respectively, with a PDI of 2.16 for PDTBBT-4F. The comparable molecular weight and dispersity values of the two copolymers excluded the effect of molecular weight on physicochemical properties and PSC device performance. As shown in Fig. S18 (ESI†), the thermal properties of PDTBBT-3F and PDTBBT-4F were next investigated by thermogravimetric analysis (TGA) to find that both copolymers present thermal decomposition temperatures (T_d) at 5% weight loss above 375 °C, indicating high thermal stability.

3.2 Optical and electrochemical properties

The UV-vis absorption spectra of PDTBBT-3F and PDTBBT-4F in diluted 1,2-dicholobenzene (*o*-DCB) solution and in film are shown in Fig. 1a. Each copolymer shows a slight redshift (~10–15 nm) in the absorption of the film relative to that of the solution. Similar spectral shapes in both solution and film can also be observed for the two copolymers at room temperature. To figure out if there exists aggregation behaviour in solution, the temperature-dependent absorption spectra were

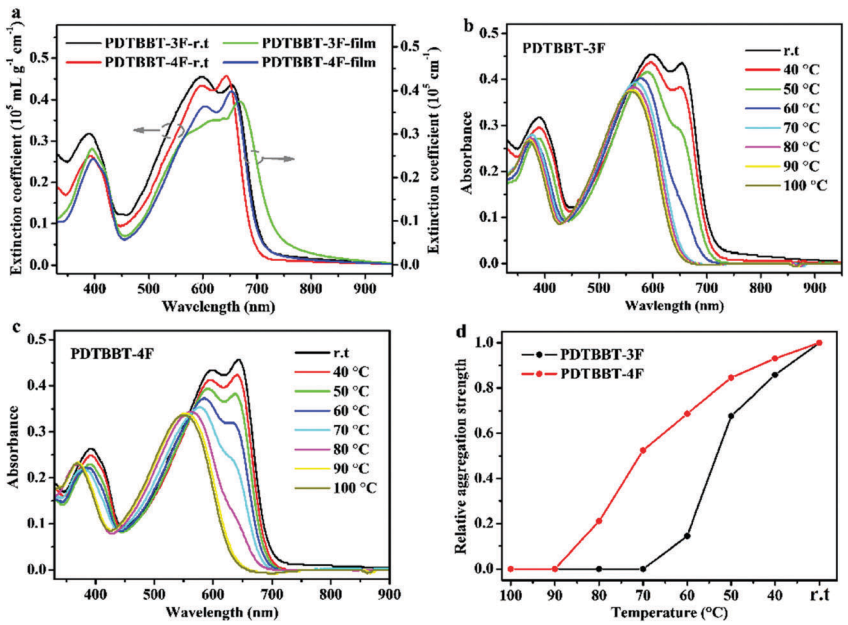

Fig. 1 (a) Absorbance coefficient spectra of PDTBBT-3F and PDTBBT-4F both in *o*-DCB solution (1×10^{-5} g mL^{-1}) and in film at room temperature; temperature-dependent UV-vis absorption spectra of 1×10^{-5} g mL^{-1} (b) PPDTBT-3F and (c) PPDTBT-4F; and (d) a plot of "relative aggregation strength" *versus* solution temperature.

Published on 04 September 2018. Downloaded by National Synchrotron Radiation Research on 1/15/2019 1:43:13 AM.

measured from room temperature to 100 °C for PDTBBT-3F and PDTBBT-4F. Fig. 1b and c indicate that PDTBBT-3F and PDTBBT-4F are fully disaggregated at 100 °C, and exhibit a maximum absorption peak at around 560 and 550 nm, respectively, with a large blue shift to their corresponding film absorption. As the temperature decreases, the absorption peaks of PDTBBT-3F and PDTBBT-4F gradually increase and red-shift. Meanwhile, a new 0–0 peak emerges at ~651 and 643 nm for PDTBBT-3F and PDTBBT-4F, respectively, indicating interchain aggregation in diluted solutions caused by strong intermolecular interactions. The temperature to induce the aggregation was found to be approximately 60 °C for PDTBBT-3F while it was determined to be 80 °C for PDTBBT-4F, implying a stronger aggregation tendency of the latter. To better understand the distinction in aggregation behaviour, the intensity of the 0–0 transition peak (at 651 nm for PDTBBT-3F and 643 nm for PDTBBT-4F) relative to the intensity of the peak absorbance at 100 °C was defined as the "relative aggregation strength" of the two polymers at different temperatures. Fig. 1d shows the relative aggregation strength plotted against the solution temperature. It is clear that the aggregation strength onset is at ~70 °C for PDTBBT-3F, whereas it is at ~90 °C for PDTBBT-4F, suggesting a stronger tendency for PDTBT-4F to aggregate in solution. Namely, increasing the degree of fluorination from 3 to 4 fluorine substituents leads to a slight blue shift in the absorption of both the solution and film and increases noncovalent interactions. In the thin film, PDTBBT-3F and PDTBBT-4F gave rise to maximum absorption wavelengths of 667 nm and 652 nm, which are bathochromic shifts of about 16 nm and 9 nm relative to the solution at room temperature, respectively. The optical band gap ($E_{g,opt}$) of PPDTBT-3F was calculated to be 1.70 eV from the absorption onset (λ_{onset} = 728 nm), slightly narrower than that of PPDTBT-4F ($E_{g,opt}$ = 1.77 eV, λ_{onset} = 698 nm).

Cyclic voltammetry (CV) was utilized to analyze the energy levels of PDTBBT-3F and PDTBBT-4F in the film state. The ferrocene/ferrocenium (Fc/Fc^+) reference was used as an internal standard, which was assigned an absolute energy of −4.8 eV *versus* vacuum level. As shown in Fig. S19 (ESI†), the oxidation onsets of PDTBBT-3F and PDTBBT-4F were measured at 0.63 and 0.76 V, and the corresponding HOMO energy levels are at −5.34 eV and −5.56 eV, respectively, according to the equation of $E_{HOMO} = -4.8 - E_{ox,onset}$. This result indicates that the PDTBBT-4F effectively decreases the HOMO level by around 0.13 eV compared to that of PDTBBT-3F when incorporating one more fluorine substituent onto the BT unit, which is beneficial for a higher V_{oc} in the resulting PSC devices. However, we were unable to attain the lowest unoccupied molecular orbital (LUMO) levels from the CV measurement due to the absence of any reductive peak. The LUMO energy levels were therefore approximately calculated as −3.73 eV for PDTBBT-3F and −3.79 eV for PDTBBT-4F from E_{HOMO} and $E_{g,opt}$ ($E_{LUMO} = E_{HOMO} + E_{g,opt}$). These results are consistent with previous reports that fluorine substitution can effectively lower the HOMO and LUMO energy levels of polymers, particularly more effectively for HOMO levels.[41,45]

3.3 Photovoltaic device characterization

Note that the polymer energy levels are appropriate to pair with $PC_{71}BM$ (Fig. 2a) for efficient photo-induced electron transfer. BHJ PSC devices of these polymers with $PC_{71}BM$ were fabricated to investigate their photovoltaic properties. The conventional device structure of ITO/PEDOT:PSS/polymer:$PC_{71}BM$/Ca/Al was adopted in this work. The active layers were spin-coated from the

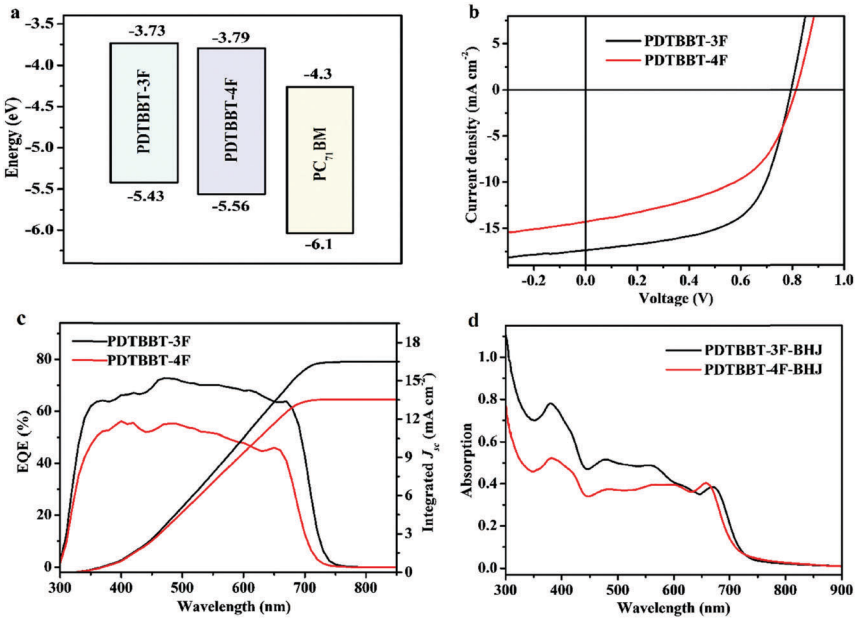

Fig. 2 (a) Energy level diagrams of the two copolymers and $PC_{71}BM$; (b) typical *J*–*V* curves under AM 1.5G irradiation; (c) EQE spectra and integrated J_{sc} curves; and (d) the absorption spectra of BHJ PSCs with the blends of PDTBBT-3F:$PC_{71}BM$ and PDTBBT-4F:$PC_{71}BM$.

 This journal is © The Royal Society of Chemistry 2018

Published on 04 September 2018. Downloaded by National Synchrotron Radiation Research on 1/15/2019 1:43:13 AM.

polymer:$PC_{71}BM$ solutions in *o*-DCB with a polymer concentration of 10 mg mL^{-1}. The optimal weight ratio of polymer:$PC_{71}BM$ was found to be 1 : 2.5 for the PDTBBT-3F:$PC_{71}BM$ blend with the film thickness about 205 nm and 1 : 2 for the PDTBBT-4F : $PC_{71}BM$ blend with the thickness around 185 nm (Fig. S20, ESI†). Corresponding photovoltaic parameters are summarized in Table S1 (ESI†). The use of processing additives can often be used to modify the BHJ morphology, resulting in the improvement of device properties in many cases.[49,50] However, lower device performance was obtained when a certain volume of solvent additives such as DIO and DPE was employed to process the BHJ blends in this contribution (Table S2, ESI†).

The photovoltaic characteristics were tested under illumination of AM 1.5G (100 mW cm^{-2}). Fig. 2b and c depict the optimized current density–voltage (*J*–*V*) curves and external quantum efficiency (EQE) spectra, respectively, while the corresponding device parameters including J_{sc}, V_{oc}, FF and PCE are summarized in Table 1. As shown in Fig. 2b, a maximum PCE of 8.33% with a V_{oc} of 0.80 V, a J_{sc} of 17.35 mA cm^{-2} and an FF of 59.8% was attained for the PDTBBT-3F device. Nevertheless, the maximum PCE dramatically decreased to 5.92% for the PDTBBT-4F device with a V_{oc} of 0.82, a J_{sc} of 14.25 mA cm^{-2} and an FF of 50.7%. As discussed in the CV experiments, the deeper HOMO energy level of PDTBBT-4F gives it a little bit higher V_{oc} in the PSC device than the PDTBBT-3F counterpart. From the EQE spectra in Fig. 2c, it is clear that the PDTBBT-3F device exhibits a higher EQE value than that of the PDTBBT-4F device over the entire absorption range. The obviously improved photocurrent response can be partly ascribed to the increased absorption of its BHJ blend film as shown in Fig. 2d. Taking into account simultaneously improved J_{sc} and FF values for PDTBBT-3F, the different light-harvesting capabilities between the two copolymers would not be the sole cause for the improvement of the J_{sc}. The morphological structures could play an important role. Briefly, the main contribution to the much higher device performance of the PDTBBT-3F device comes from much improved J_{sc} and FF compared with those of the PDTBBT-4F device.

3.4 Charge generation, transport and recombination

The analysis of charge generation, transport and recombination behaviours is useful to better understand the divergence in the photovoltaic performance, especially J_{sc} and FF, between the PDTBBT-3F:$PC_{71}BM$ and PDTBBT-4F:$PC_{71}BM$ devices. Firstly, the maximum photoinduced carrier generation rates (G_{max}) were determined to compare exciton generation and dissociation by investigating the photocurrent density (J_{ph}) as a function of the effective voltage (V_{eff}) between both devices. J_{ph} is determined as $J_{ph} = J_L - J_D$, where J_L and J_D represent the photocurrent densities under illumination and in the dark, respectively.[51] Meanwhile, V_{eff} is defined as $V_{eff} = V_0 - V_{appl}$, where V_0 is the built-in voltage when J_{ph} equals zero and V_{appl} is the applied voltage. As shown in Fig. 3a, J_{ph} gradually increases at low V_{eff} and then reaches saturation at a sufficiently high value about 1.3 V and above, where all photogenerated excitons dissociate and collect at the corresponding electrode. G_{max} can be calculated *via* the equation $G_{max} = J_{ph,sat}/qL$, where $J_{ph,sat}$ is the saturated photocurrent density, q is the electric charge, and L is the thickness of the active layer. The G_{max} for the device with PDTBBT-3F is determined to be 0.55×10^{28} m^{-3} s^{-1} ($J_{ph,sat}$ = 180.5 A m^{-2}) while it decreases to 0.52×10^{28} m^{-3} s^{-1} ($J_{ph,sat}$ = 156.8 A m^{-2}) for the device with PDTBBT-4F. Such slight enhancement in G_{max} for the PDTBBT-3F device could be partially attributed to the enhanced extinction coefficient in 300–550 nm (Fig. S21, ESI†). Moreover, the exciton dissociation probabilities ($P_{(E,T)}$), defined as $P_{(E,T)} = J_{ph}/J_{ph,sat}$, were calculated to be 96.1% for the PDTBBT-3F device under the short circuit current condition ($J_{ph} = J_{sc}$ at V_{appl} = 0 V), which is much higher than 90.8% for the PDTBBT-4F device. The higher $P_{(E,T)}$ for PDTBBT-3F can also be proved by photoluminescence (PL) quenching of the BHJ blends. Fig. 3b displays the PL spectra of PDTBBT-3F and PDTBBT-4F and their blend films with $PC_{71}BM$ excited at 670 nm and 660 nm, respectively. Relative to the neat polymer films, a quenching efficiency of 96.5% was obtained for the PDTBBT-3F device whereas it was only 89.3% in the PDTBBT-4F blend film, suggesting more efficient photo induced charge transfer within the PDTBBT-3F:$PC_{71}BM$ blend. In addition, it can also be observed from the inset of Fig. 3a that the PDTBBT-3F device exhibits a lower leakage current of the diode with a higher ratification factor of approximately six times relative to the PDTBBT-4F device at reverse bias, indicating improved film quality.

The improvement of $P_{(E,T)}$ and the PL quenching efficiency for the PDTBBT-3F device illustrates that geminate recombination was more effectively suppressed compared to devices with PDTBBT-4F. Besides the geminate recombination, non-geminate recombination (bimolecular recombination and monomolecular recombination) is proportional to the carrier mobility in the process of charge transport. The charge recombination mechanism in the BHJ blends of PDTBBT-3F and PDTBBT-4F was therefore explored by measuring the *J*–*V* curves responding to gradually increased incident light intensity (P_{light}).[52] Fig. 3c exhibits the logarithmic plots of J_{sc} as a function of the light intensity and the data were fitted to the power law: $J_{sc} \propto (P_{light})^{\alpha}$, where the closer the α value to 1, the less bimolecular

Table 1 Summary of device parameters for the optimized polymer:$PC_{71}BM$ blends in a conventional device configuration under AM 1.5G illumination

Polymer	D : A ratio	Thickness[a] (nm)	V_{oc} (V)	J_{sc} (mA cm^{-2})	FF (%)	PCE[b] (%)
PDTBBT-3F	1 : 2.5	205 ± 3	0.804 (0.798 ± 0.009)	17.35 (17.12 ± 0.30)	59.8 (59.4 ± 0.9)	8.33 (8.15 ± 0.21)
PDTBBT-4F	1 : 2	185 ± 2	0.817 (0.812 ± 0.007)	14.25 (14.03 ± 0.24)	50.7 (50.3 ± 1.0)	5.92 (5.79 ± 0.16)

[a] The average values and standard deviations from 6 devices. [b] The average values and standard deviations are shown in parentheses from 15 devices.

Published on 04 September 2018. Downloaded by National Synchrotron Radiation Research on 1/15/2019 1:43:13 AM.

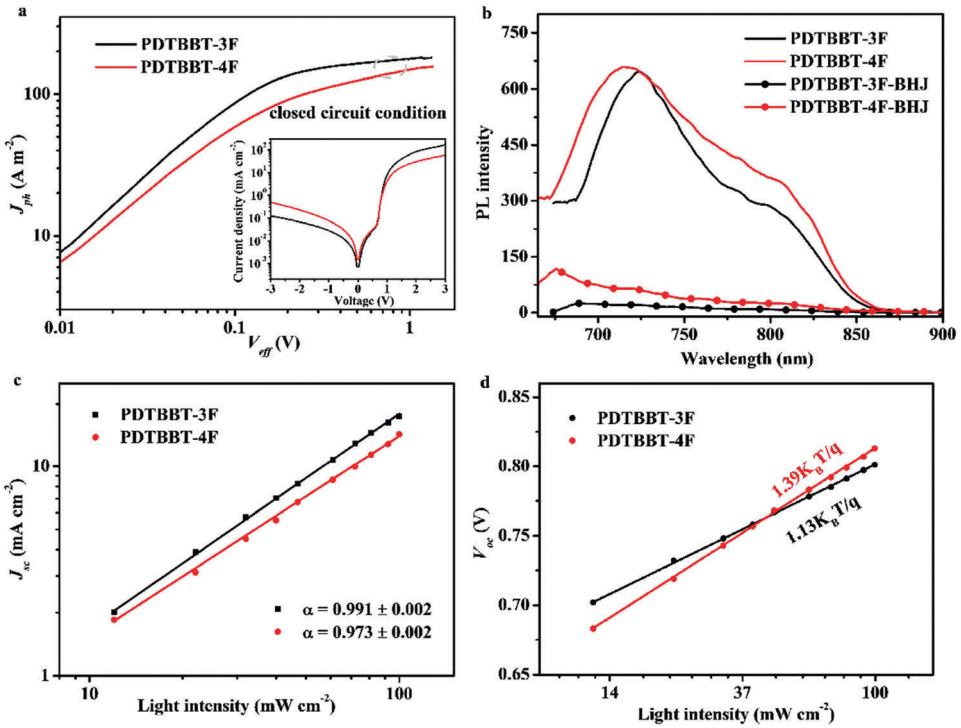

Fig. 3 (a) Photogenerated current density *versus* effective voltage curves under AM 1.5G illumination (the inset shows dark current J–V curves from −3 V to +3 V); (b) photoluminescence spectra of neat polymer films and their BHJ blends excited at 670 nm and 660 nm for PDTBBT-3F and PDTBBT-4F, respectively; and (c) dependence of J_{sc} on light intensity and (d) dependence of V_{oc} on light intensity within the BHJ PSCs containing PDTBBT-3F and PDTBBT-4F.

recombination, suggesting most of the free charge carriers can be collected at the corresponding electrodes before recombination. A relatively larger α value (0.991) was obtained for the PDTBBT-3F:$PC_{71}BM$ blend compared to PDTBBT-4F (0.973), suggesting that bimolecular recombination was suppressed. Meanwhile, measurement of V_{oc} as a function of P_{light} was carried out as well to probe monomolecular recombination within the devices. Fig. 3d presents a semilogarithmic plot of V_{oc} as a function of P_{light} and the curves were fitted according to the law $V_{oc} \propto (nk_BT/q)\ln(P_{light})$, where k_B is the Boltzmann constant (1.38×10^{-23} J K^{-1}), T is temperature in Kelvin, and q is the elementary charge (1.6×10^{-19} C). The slope for PDTBBT-3F and PDTBBT-4F was calculated to be $1.13k_BT/q$ and $1.39k_BT/q$, respectively. The smaller n value for PDTBBT-3F indicates lower monomolecular recombination. These data indicate that the PDTBBT-3F:$PC_{71}BM$ PSC can sweep out charge carriers more efficiently with negligible non-geminate recombination compared to the PDTBBT-4F:$PC_{71}BM$ PSC.

Vertical charge carrier mobilities of both PSCs were measured by the space charge limited current (SCLC) method using ITO/ZnO/polymer:$PC_{71}BM$/Ca/Al and ITO/PEDOT:PSS/polymer:$PC_{71}BM$/MoO_3/Ag as the corresponding electron-only and hole-only devices. As shown in Fig. S22 (ESI†), the hole mobilities (μ_h) were calculated to be 5.65×10^{-4} cm^2 V^{-1} s^{-1} and 4.18×10^{-4} cm^2 V^{-1} s^{-1} for the PDTBBT-3F and PDTBBT-4F blend films, and the corresponding electron mobilities (μ_e) are 4.12×10^{-4} cm^2 V^{-1} s^{-1} and 0.87×10^{-4} cm^2 V^{-1} s^{-1}, respectively. Obviously, compared to the PDTBBT-4F device, the PDTBBT-3F:$PC_{71}BM$ blend presents a slightly enhanced hole mobility and a higher electron mobility. Therefore, the lower electron mobility within the PDTBBT-4F:$PC_{71}BM$ blend film would destroy the balance of charge transport (μ_h/μ_e = 4.80) compared to that of PDTBBT-3F:$PC_{71}BM$ (μ_h/μ_e = 1.37) and then increase charge recombination on the way to the electrodes as verified above. Less balance of charge transport could be one of the reasons for the low FF and the limited PCE in the device with PDTBBT-4F.

3.5 Structure characterization of neat polymer and BHJ blend films

Given the fact that PDTBBT-4F presents not only comparable solubility but also a similar TDA property to that of PDTBBT-3F, its inferior device performance, especially in J_{sc} and FF, sparked our strong curiosity due to stronger intermolecular interactions in PDTBBT-4F. Film morphology has been proven to play a determinant role in governing each photoelectric conversion step such as charge generation, recombination, transportation and collection. Distinctive film microstructures could be presented between the two copolymers and their BHJ blends due to variable aggregation strength triggered by the degree of multi-fluorination. Grazing incidence wide-angle X-ray scattering (GIWAXS) measurements were performed to gain a deeper understanding of the molecular orientation and crystallinity of the neat and BHJ blend films. Fig. 4 shows the GIWAXS diffraction patterns and the corresponding profiles of the neat polymers and their corresponding BHJ blends along both the out of plane (OOP) and in plane (IP) directions.

 This journal is © The Royal Society of Chemistry 2018

Published on 04 September 2018. Downloaded by National Synchrotron Radiation Research on 1/15/2019 1:43:13 AM.

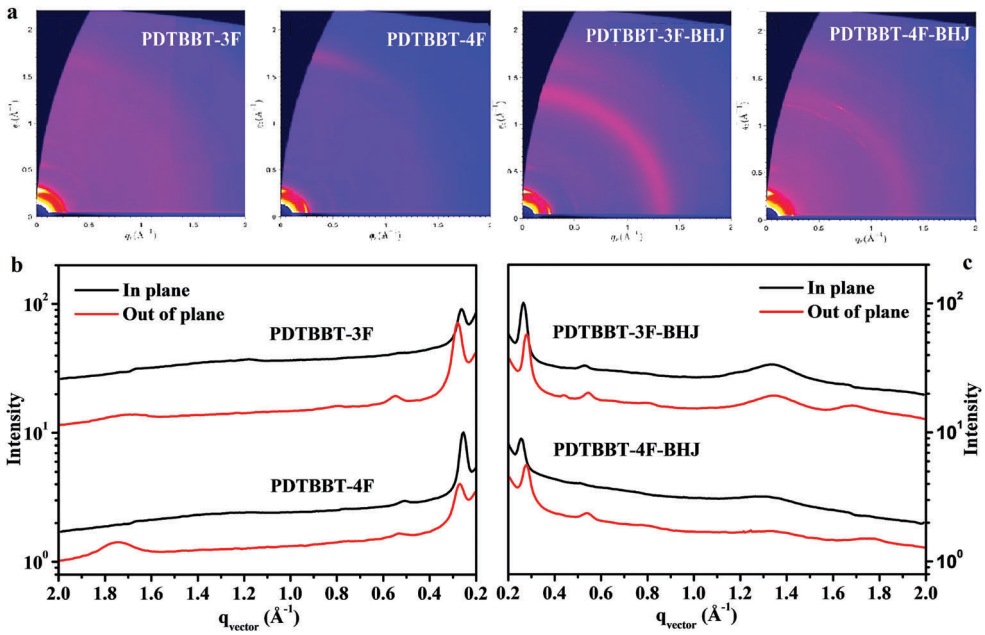

Fig. 4 2D GIWAXS patterns of the neat polymer films and the polymer:$PC_{71}BM$ BHJ blend films (a) and scattering profiles along the in-plane (IP) and out-of plane (OOP) directions for the neat PDTBBT-3F and PDTBBT-4F films (b) and for the polymer:$PC_{71}BM$ BHJ blend films (c).

As shown in Fig. 4b, both copolymers exhibit an obvious edge-on/face on intermixed orientation of crystalline lamellae. Notably, the relative proportion between edge-on and face-on orientated crystalline lamellae is found to be diametrically opposite between PDTBBT-3F and PDTBBT-4F due to the different degree of multi-fluorination. For the neat PDTBBT-3F, a weaker lamellar IP (100) diffraction at q_r of 0.264 Å^{-1} with a distance (d) of 23.78 Å and a coherence length (L_c) of 120.5 Å corresponding to alkyl side chain stacking in the in-plane direction is observed. Additionally, the neat PDTBBT-3F film shows an OOP π–π stacking (010) diffraction at q_z of around 1.702 Å^{-1} (d = 3.69 Å) with a L_c of 21.2 Å. A stronger OOP lamellar diffraction (100) peak at 0.280 Å^{-1} with a d space of 22.43 Å and a L_c of 148.1 Å is observed as well, indicating that the edge-on orientation is the mild preference in this film. However, the neat PDTBBT-4F film forms crystalline lamellae with preferential face-on orientated molecular packing, which is evidenced by the existence of a stronger IP lamellar diffraction (100) at q_r of 0.258 Å^{-1} (d = 24.34 Å) with a larger L_c of 164.4 Å and a sharp OOP (010) π–π stacking diffraction at q_z of around 1.747 Å^{-1} (d = 3.59 Å) with a L_c of 36.8 Å. Meanwhile, a weaker OOP lamellar stacking (100) diffraction at q_z of around 0.270 Å^{-1} (d = 23.26 Å) with a L_c of 108.3 Å can be found as well although without a corresponding obvious IP (010) π–π stacking diffraction. Interestingly, when compared with the PDTBBT-3F film, the lamellar spacings of both IP and OOP (100) diffractions are accordingly a little bit larger in PDTBBT-4F while the observed OOP (010) π–π stacking is more compact. These results suggest that adding one more fluorine onto the conjugated backbone induces the formation of face-on orientated polymer crystals in PDTBBT-4F, which can be attributed to its increased backbone planarity and improved intermolecular interaction as demonstrated by the observation of its stronger interchain aggregation in diluted solution.

Surprisingly, when blended with $PC_{71}BM$ to form BHJ blend films, a transformation in the molecular packing orientation occurred once again between the two copolymers. As depicted in Fig. 4c, although the intermixed edge-on/face on orientation remains for both copolymers in their BHJ blends, the relative proportions of both orientations and crystallinity are turned. Both copolymers exhibit similar lamellar distances of around 24.15 Å and 22.43 Å along the IP and OOP direction in the BHJ blends, respectively. In the PDTBBT-3F:$PC_{71}BM$ blend, face-on orientated polymer crystals are strengthened while edge-on orientated crystals are decreased until both reach comparable intensity between the IP (100) and OOP (100) diffractions in comparison with the neat film of PDTBBT-3F, suggesting more balanced lamellar stacking along both the IP and OOP directions after its blend with $PC_{71}BM$. In contrast, face-on orientated polymer crystals are suppressed to be comparable with edge-on orientated ones in the PDTBBT-4F:$PC_{71}BM$ blend film compared with the neat PDTBBT-4F film with preferential face-on orientation. Moreover, the coherence lengths (Table S4, ESI†) corresponding to the (100) diffractions in both IP and OOP directions and the OOP (010) diffraction of PDTBBT-3F are improved in the PDTBBT-3F:$PC_{71}BM$ blend film in comparison with the counterpart of PDTBBT-4F, suggesting higher crystallinity for PDTBBT-3F and more ordering within the BHJ film. The characteristic diffraction at around 1.33 Å^{-1} corresponding to $PC_{71}BM$ aggregations becomes more ordered with higher crystallinity in the PDTBBT-3F:$PC_{71}BM$ blend compared to that of the PDTBBT-4F:$PC_{71}BM$ blend, explaining the higher electron mobility in the PDTBBT-3F:$PC_{71}BM$ device. This result indicates that the relatively stronger aggregation behaviour of PDTBBT-4F

Published on 04 September 2018. Downloaded by National Synchrotron Radiation Research on 1/15/2019 1:43:13 AM.

in solution, deduced from its stronger intermolecular interaction, could impede efficient D–A miscibility between PDTBBT-4F and $PC_{71}BM$ while it is opposite in the PDTBBT-3F case. Such distinct intermolecular interaction between the electron donor and acceptor within the BHJ blends in turn induced significantly different molecular packing orientation and crystallinity. The more balanced intermixing of edge-on/face-on orientated crystals with higher crystallinity of PDTBBT-3F and better ordering of $PC_{71}BM$ aggregation within the BHJ blend could facilitate charge generation and transport and suppress charge recombination, thus leading to improved J_{sc} and FF.

The surface morphology of the BHJ blends was also investigated by tapping-mode atomic force microscopy (AFM) as shown in Fig. S23 (ESI†). The PDTBBT-3F:$PC_{71}BM$ blend film exhibits a relatively smooth surface with a root-mean-square (RMS) roughness of 4.77 nm compared to the 8.68 nm of the PDTBT-4F device, indicating good miscibility between the donor and acceptor components. Moreover, well-distributed fibrillar structures from the phase image of the PDTBBT-3F device can also be observed, which could also be beneficial to exciton dissociation and charge transport. However, the PDTBBT-4F:$PC_{71}BM$ blend film exhibits more phase separation, with larger aggregation domains, which may be attributed to the stronger intermolecular interaction of PDTBBT-4F. This result partially supports the proposal mentioned above that larger aggregation hinders the miscibility of the PDTBBT-4F with $PC_{71}BM$ within the BHJ blend.

4. Conclusions

In summary, two multi-fluorinated D–A copolymer donors of PDTBBT-3F and PDTBBT-4F by fluorinating both the D and A units in the same conjugated backbone bearing the same alkyl side chains were employed to investigate the effect of multi-fluorination on molecular packing and the resultant photovoltaic performance. In spite of the similar solubility in the processing solvent, the addition of another fluorine substitution further increases the intermolecular interaction and temperature-dependent-aggregation behaviour for PDTBBT-4F compared to PDTBBT-3F. In neat polymer films, PDTBBT-4F prefers a face-on molecular packing compared with the edge-on morphology for PDTBBT-3F. The stronger intermolecular interaction of PDTBBT-4F impeded efficient D–A miscibility between PDTBBT-4F and $PC_{71}BM$. Such varied intermolecular interactions within the BHJ blends in turn gave PDTBBT-3F uniform intermixing of edge-on/face-on orientation with improved crystallinity and ordering, while PDTBBT-4F evolved oppositely into a mixed edge-on/face-on orientation with less crystallinity and coherence. A much higher device efficiency of 8.33% was therefore achieved from the PDTBBT-3F:$PC_{71}BM$ device with around a 40% increase compared to that of PDTBBT-4F:$PC_{71}BM$ (5.92%), mainly by promoting J_{sc} and FF due to the enhancement of charge generation and transport and the oppression of charge recombination within the device. These results begin to disclose the underlying causes for the distinction in molecular packing and photovoltaic properties between multi-fluorinated copolymers conveyed by the degree of fluorination. This research provides meaningful guidance on selective fluorination of electron donors for higher device performance.

Conflicts of interest

There are no conflicts to declare.

Acknowledgements

S. Xiao thanks the support from National Natural Science Foundation of China (21673170).

Notes and references

1 G. Yu, J. Gao, J. C. Hummelen, F. Wudl and A. J. Heeger, *Science*, 1995, **270**, 1789.
2 R. Søndergaard, M. Hösel, D. Angmo, T. T. Larsen-Olsen and F. C. Krebs, *Mater. Today*, 2012, **15**, 36.
3 H. Kang, G. Kim, J. Kim, S. Kwon, H. Kim and K. Lee, *Adv. Mater.*, 2016, **28**, 7821.
4 L. Lu, T. Zheng, Q. Wu, A. M. Schneider, D. Zhao and L. Yu, *Chem. Rev.*, 2015, **115**, 12666.
5 Y. Cai, L. Huo and Y. Sun, *Adv. Mater.*, 2017, **29**, 1605437.
6 S. Xiao, Q. Zhang and W. You, *Adv. Mater.*, 2017, **29**, 1601391.
7 C. Liu, K. Wang, X. Gong and A. J. Heeger, *Chem. Soc. Rev.*, 2016, **45**, 4825.
8 K. A. Mazzio and C. K. Luscombe, *Chem. Soc. Rev.*, 2015, **44**, 78.
9 L. Lu, M. A. Kelly, W. You and L. Yu, *Nat. Photonics*, 2015, **9**, 491.
10 H. Huang, L. Yang and B. Sharma, *J. Mater. Chem. A*, 2017, **5**, 11501.
11 W. Cai, X. Gong and Y. Cao, *Sol. Energy Mater. Sol. Cells*, 2010, **94**, 114.
12 H. Yao, Y. Li, H. Hu, P. C. Y. Chow, S. Chen, J. Zhao, Z. Li, J. H. Carpenter, J. Y. L. Lai, G. Yang, Y. Liu, H. Lin, H. Ade and H. Yan, *Adv. Energy Mater.*, 2018, **8**, 1701895.
13 S. Li, L. Ye, W. Zhao, H. Yan, B. Yang, D. Liu, W. Li, H. Ade and J. Hou, *J. Am. Chem. Soc.*, 2018, **140**, 7159.
14 J. Zhao, Y. Li, G. Yang, K. Jiang, H. Lin, H. Ade, W. Ma and H. Yan, *Nat. Energy*, 2016, **1**, 15027.
15 S. Zhang, Y. Qin, J. Zhu and J. Hou, *Adv. Mater.*, 2018, **30**, 1800868.
16 Z. Xiao, J. Xue and L. Ding, *Sci. Bull.*, 2017, **62**, 1562.
17 C. McDowell, M. Abdelsamie, M. F. Toney and G. C. Bazan, *Adv. Mater.*, 2018, **30**, 1707114.
18 M. He, M. Wang, C. Lin and Z. Lin, *Nanoscale*, 2014, **6**, 3984.
19 B. C. Thompson and J. M. J. Fréchet, *Angew. Chem., Int. Ed.*, 2008, **47**, 58.
20 M. E. Ziffer, S. B. Jo, H. Zhong, L. Ye, H. Liu, F. Lin, J. Zhang, X. Li, H. W. Ade, A. K. Y. Jen and D. S. Ginger, *J. Am. Chem. Soc.*, 2018, **140**, 9996.

 This journal is © The Royal Society of Chemistry 2018

Published on 04 September 2018. Downloaded by National Synchrotron Radiation Research on 1/15/2019 1:43:13 AM.

21 C. S. Ponseca, P. Chábera, J. Uhlig, P. Persson and V. Sundström, *Chem. Rev.*, 2017, **117**, 10940.
22 H. Sun, X. Song, J. Xie, P. Sun, P. Gu, C. Liu, F. Chen, Q. Zhang, Z.-K. Chen and W. Huang, *ACS Appl. Mater. Interfaces*, 2017, **9**, 29924.
23 W. Chen, X. Yang, G. Long, X. Wan, Y. Chen and Q. Zhang, *J. Mater. Chem. C*, 2015, **3**, 4698.
24 B. Cao, L. A. Adutwum, A. O. Oliynyk, E. J. Luber, B. C. Olsen, A. Mar and J. M. Buriak, *ACS Nano*, 2018, **12**, 7434.
25 H. Zhou, L. Yang and W. You, *Macromolecules*, 2012, **45**, 607–632.
26 R. L. Uy, S. C. Price and W. You, *Macromol. Rapid Commun.*, 2012, **33**, 1162.
27 Y. Ma, Z. Kang and Q. Zheng, *J. Mater. Chem. A*, 2017, **5**, 1860–1872.
28 J. Yuan, J. Ouyang, V. Cimrová, M. Leclerc, A. Najari and Y. Zou, *J. Mater. Chem. C*, 2017, **5**, 1858.
29 H. Yao, L. Ye, H. Zhang, S. Li, S. Zhang and J. Hou, *Chem. Rev.*, 2016, **116**, 7397.
30 J.-S. Wu, S.-W. Cheng, Y.-J. Cheng and C.-S. Hsu, *Chem. Soc. Rev.*, 2015, **44**, 1113.
31 H. Hu, P. C. Y. Chow, G. Zhang, T. Ma, J. Liu, G. Yang and H. Yan, *Acc. Chem. Res.*, 2017, **50**, 2519.
32 F. Meyer, *Prog. Polym. Sci.*, 2015, **47**, 70.
33 Q. Zhang, M. A. Kelly, N. Bauer and W. You, *Acc. Chem. Res.*, 2017, **50**, 2401.
34 X.-P. Xu, Y. Li, M.-M. Luo and Q. Peng, *Chin. Chem. Lett.*, 2016, **27**, 1241.
35 N. Leclerc, P. Chávez, O. Ibraikulov, T. Heiser and P. Lévêque, *Polymers*, 2016, **8**, 11.
36 K. Kranthiraja, S. Kim, C. Lee, K. Gunasekar, V. G. Sree, B. Gautam, K. Gundogdu, S.-H. Jin and B. J. Kim, *Adv. Funct. Mater.*, 2017, **27**, 1701256.
37 P. Chen, S. Shi, H. Wang, F. Qiu, Y. Wang, Y. Tang, J.-R. Feng, H. Guo, X. Cheng and X. Guo, *ACS Appl. Mater. Interfaces*, 2018, **10**, 21481.
38 A. C. Stuart, J. R. Tumbleston, H. Zhou, W. Li, S. Liu, H. Ade and W. You, *J. Am. Chem. Soc.*, 2013, **135**, 1806.
39 C. J. Mueller, E. Gann, C. R. McNeill and M. Thelakkat, *J. Mater. Chem. C*, 2015, **3**, 8916.
40 Y. Zhang, S.-C. Chien, K.-S. Chen, H.-L. Yip, Y. Sun, J. A. Davies, F.-C. Chen and A. K. Y. Jen, *Chem. Commun.*, 2011, **47**, 11026.
41 I.-B. Kim, S.-Y. Jang, Y.-A. Kim, R. Kang, I.-S. Kim, D.-K. Ko and D.-Y. Kim, *ACS Appl. Mater. Interfaces*, 2017, **9**, 24011.
42 O. A. Ibraikulov, R. Bechara, P. Chavez, I. Bulut, D. Tastanbekov, N. Leclerc, A. Hebraud, B. Heinrich, S. Berson, N. Lemaitre, C. L. Chochos, P. Lévêque and T. Heiser, *Org. Electron.*, 2015, **23**, 171.
43 O. A. Ibraikulov, C. Ngov, P. Chávez, I. Bulut, B. Heinrich, O. Boyron, K. L. Gerasimov, D. A. Ivanov, S. Swaraj, S. Méry, N. Leclerc, P. Lévêque and T. Heiser, *J. Mater. Chem. A*, 2018, **6**, 12038.
44 K. Kawashima, T. Fukuhara, Y. Suda, Y. Suzuki, T. Koganezawa, H. Yoshida, H. Ohkita, I. Osaka and K. Takimiya, *J. Am. Chem. Soc.*, 2016, **138**, 10265.
45 S.-J. Ko, Q. V. Hoang, C. E. Song, M. A. Uddin, E. Lim, S. Y. Park, B. H. Lee, S. Song, S.-J. Moon, S. Hwang, P.-O. Morin, M. Leclerc, G. M. Su, M. L. Chabinyc, H. Y. Woo, W. S. Shin and J. Y. Kim, *Energy Environ. Sci.*, 2017, **10**, 1443.
46 J. W. Jo, J. W. Jung, E. H. Jung, H. Ahn, T. J. Shin and W. H. Jo, *Energy Environ. Sci.*, 2015, **8**, 2427.
47 Z. Li, H. Lin, K. Jiang, J. Carpenter, Y. Li, Y. Liu, H. Hu, J. Zhao, W. Ma, H. Ade and H. Yan, *Nano Energy*, 2015, **15**, 607.
48 T. L. Nguyen, H. Choi, S. J. Ko, M. A. Uddin, B. Walker, S. Yum, J. E. Jeong, M. H. Yun, T. J. Shin, S. Hwang, J. Y. Kim and H. Y. Woo, *Energy Environ. Sci.*, 2014, **7**, 3040.
49 J. Peet, N. S. Cho, S. K. Lee and G. C. Bazan, *Macromolecules*, 2008, **41**, 8655.
50 C. Piliego, T. W. Holcombe, J. D. Douglas, C. H. Woo, P. M. Beaujuge and J. M. J. Fréchet, *J. Am. Chem. Soc.*, 2010, **132**, 7595.
51 A. K. K. Kyaw, D. H. Wang, V. Gupta, W. L. Leong, L. Ke, G. C. Bazan and A. J. Heeger, *ACS Nano*, 2013, **7**, 4569.
52 J. Gao, W. Wang, S. Zhang, S. Xiao, C. Zhan, M. Yang, X. Lu and W. You, *J. Mater. Chem. A*, 2018, **6**, 179.